ACS APPLIED MATERIALS & INTERFACES

Research Article

www.acsami.org

Aqueous Nanoparticle Polymer Solar Cells: Effects of Surfactant Concentration and Processing on Device Performance

Fallon J. M. Colberts,[‡] Martijn M. Wienk,[‡,†] and René A. J. Janssen*[,‡,†]

[‡]Molecular Materials and Nanosystems, Institute for Complex Molecular Systems, Eindhoven University of Technology, P.O. Box 513, 5600 MB, Eindhoven, The Netherlands

[†]Dutch Institute for Fundamental Energy Research, De Zaale 20, 5612 AJ, Eindhoven, The Netherlands

Supporting Information

ABSTRACT: Polymer solar cells based on PDPP5T and PCBM as donor and acceptor materials, respectively, were processed from aqueous nanoparticle dispersions. Careful monitoring and optimization of the concentration of free and surface-bound surfactants in the dispersion, by measuring the conductivity and ζ-potential, is essential to avoid aggregation of nanoparticles at low concentration and dewetting of the film at high concentration. The surfactant concentration is crucial for creating reproducible processing conditions that aid in further developing aqueous nanoparticle processed solar cells. In addition, the effects of adding ethanol, of aging the dispersion, and of replacing [60]PCBM with [70]PCBM to enhance light absorption were studied. The highest power conversion efficiencies (PCEs) obtained are 2.0% for [60]PCBM and 2.4% for [70]PCBM-based devices. These PCEs are limited by bimolecular recombination of photogenerated charges. Cryo-TEM reveals that the two components phase separate in the nanoparticles, forming a PCBM-rich core and a PDPP5T-rich shell and causing a nonoptimal film morphology.

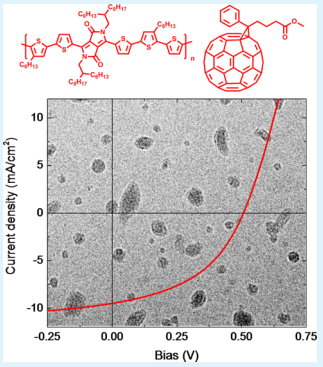

KEYWORDS: *organic photovoltaics, semiconducting polymer, fullerene, miniemulsion, nanoparticle dispersion, surfactant, ζ-potential, conductivity*

1. INTRODUCTION

Organic photovoltaics (OPV) have attracted considerable interest in the past decade as a sustainable future energy source. One of its virtues is the ability to process the photoactive layers from solutions or inks, which enables high throughput printing and roll-to-roll coating, reducing the fabrication costs and giving the opportunity to use flexible substrates.[1,2] Furthermore, advantages as light weight, thinness, semitransparency, and color tunability make OPV attractive for modern life applications.[3−5] Driven by these benefits, considerable research efforts have been dedicated to improving the performance of OPV devices, resulting in numerous new semiconducting polymers with high charge carrier mobility and optimized energy alignment.[6,7] Combined with a better understanding of the effect of polymer structure and processing on the electron donor−electron acceptor bulk heterojunction (BHJ) morphology, the power conversion efficiency (PCE) of OPVs has increased to exceed 11% for single-junction solar cells.[8−10] However, the vast majority of record efficiency solar cells have been processed from chlorinated solvents such as chlorobenzene, 1,2-dichlorobenzene (*o*-DCB), or chloroform, which are harmful to people's health and environment.[11−15] Processing the active layer from nonchlorinated solvents requires new insights and efforts to control the morphology.[10,16]

An ecofriendly strategy to use high-performance solar cell materials is their precipitation in ethanol, as has been reported by Gartner et al.[17] and Sankaran et al.[18] for solar cells based on poly(3-hexylthiophene) (P3HT) and indene-C_{60} bisadduct (ICBA). These provide PCEs over 4%; however, the method seems sensitive to the specific material combination used because such high PCEs have not yet been achieved for other materials. An alternative method is the miniemulsion technique introduced by Landfester for conjugated materials.[19] The advantages of this method are that (i) nanoparticles (NPs) can be made in the most ecofriendly solvent that exists, namely water, (ii) the NPs are stabilized, which may offer the benefit of using a variety of material combinations, and (iii) the nanoscale morphology is fixed in a single nanoparticle in a prestadium of depositing the active layer.

The PCEs of aqueous minielemusion NP solar cells are less than those of conventional BHJs, e.g. when using a photoactive layer based on P3HT and [6,6]-phenyl-C_{61}-butyric acid methyl ester ([60]PCBM). The thermal annealing of the active layer, which is essential to merge the aqueous NPs, also cause P3HT and [60]PCBM to crystallize and form large donor and acceptor domains that lower the performance.[20,21] A comparison between P3HT that crystallizes under thermal treatment and a polymer that is crystalline as spun has been reported by Dam et al., where NPs have been synthesized from P3HT:[60]PCBM and poly[4,8-bis(2-ethylhexyloxy)benzo-(1,2-b:4,5-b′)dithiophene-*alt*-5,6-bis(octyloxy)-4,7-di-

Received: January 12, 2017
Accepted: March 27, 2017
Published: March 27, 2017

DOI: 10.1021/acsami.7b00557
ACS Appl. Mater. Interfaces 2017, 9, 13380−13389

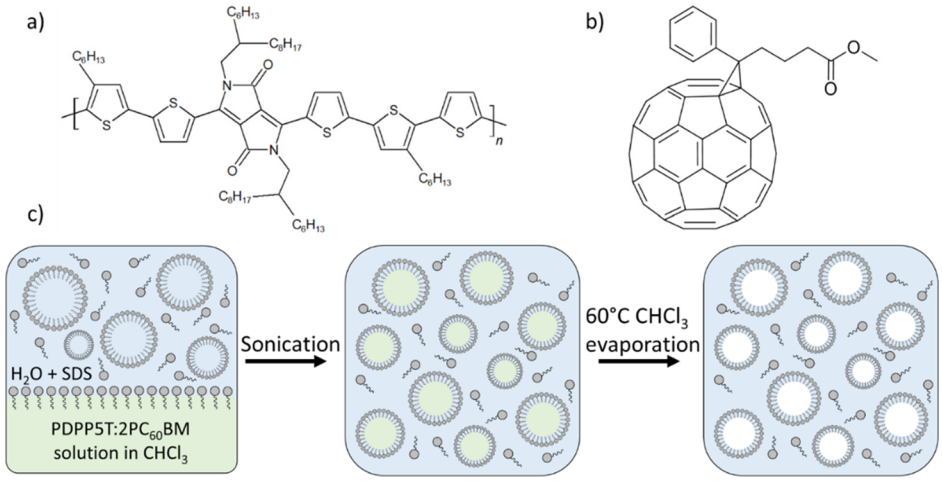

Figure 1. Molecular structures of (a) PDPP5T and (b) [60]PCBM. (c) Principle of the miniemulsion method.

(thiophen-2-yl) (2,1,3-benzothiadiazole)-5,5′-diyl] (PSBTBT):[60]PCBM.[22] Scanning transmission X-ray microscopy (STXM) showed that in both cases a core−shell morphology was formed where the core was [60]PCBM-rich and the shell polymer-rich. This phase separation was attributed to the high and very similar water contact angle of the polymers compared to that of [60]PCBM. Dam et al. showed that the shell constituted >80% of the total NP volume and that a higher PCE can be obtained relative to the BHJ performance when the shell composition is closer to the optimized BHJ composition. According to Holmes et al. the shell composition can be optimized by varying the polymer:[60]PCBM ratio.[21] Instead of using rather crystalline donor polymers such as P3HT and PSBTBT, Holmes et al. reported working NP solar cells based on the amorphous polymer poly[2,3-bis(3-octyloxyphenyl)-quinoxaline-5,8-diyl-*alt*-thiophene-2,5-diyl] (TQ1) in combination with [6,6]-phenyl-C_{71}-butylric acid methyl ester ([70]-PCBM).[23] The high glass transition temperature of TQ1 (T_g ∼ 100 °C) with respect to that of P3HT (T_g ∼ 12 °C)[24] prevents phase separation upon mild thermal annealing of the active layer.[23] Also for this material combination, a core−shell morphology was observed by STXM and transmission electron microscopy (TEM). Thermal treatment above the glass transition temperature of the polymer-rich shell allowed the shells of neighboring particles to merge together and [70]PCBM to locally diffuse. Optimization of the annealing conditions resulted in an optimized morphology with connecting pathways between the [70]PCBM-rich cores. These TQ1:[70]PCBM solar cells gave a PCE of 2.54%.

In contrast to the often-obtained core−shell morphology, D'Olieslaeger et al. reported that poly([9-(1′-octylnonyl)-9*H*-carbazole-2,7-diyl]-2,5-thiophenediyl-2,1,3-benzothiadiazole-4,7-diyl-2,5-thiophene-diyl) (PCDTBT):[70]PCBM NPs do not show a phase-separated morphology.[25] This has been confirmed by TEM and scanning TEM (STEM) in combination with electron energy-loss spectroscopy. Recently, D'Olieslaeger et al. achieved a PCE of 3.8% utilizing poly[(5,6-dihydro-5-octyl-4,6-dioxo-4*H*-thieno[3,4-*c*]pyrrole-1,3-diyl)-[4,8-bis[(2-ethylhexyl)oxy]benzo[1,2-b:4,5-b′]dithiophene-2,6-diyl]] (PBDTTPD):[70]PCBM, which is the highest performance reported for aqueous NP solar cells to date.[26]

In this work, we investigate aqueous NP dispersions of a diketepyrrolopyrrole−quinquethiophene alternating copolymer (PDPP5T) and [60]PCBM (Figure 1), prepared via the miniemulsion method. PDPP5T is an example of a modern semicrystalline small band gap polymer exhibiting a relatively good PCE of 6% in regular BHJ blends with fullerenes. We have extensively studied morphology formation for PDPP5T−fullerene mixtures for conventional BHJ blends.[27] This allows for a direct comparison with layers obtained from aqueous nanoparticle dispersions. We demonstrate that the surfactant concentration in the dispersion is a critical parameter that must be optimized in film formation to balance between aggregation of NPs at low concentration and film dewetting at a high concentration. The amount of free and surface-bound surfactant in the dispersion can be monitored via the conductivity and ζ-potential, which improved the reproducibility of the solar cells with a performance of ∼1.5% when properly controlled. The PCE can be improved to approximately 2.0% by aging the dispersion or adding ethanol. By replacing [60]PCBM with [70]PCBM, a further increase of PCE to 2.4% is achieved. The main limitation of the NP photoactive later is the extent of bimolecular recombination, which leads to a low short-circuit current density (J_{SC}) and fill factor (FF). Cryo-TEM was used to analyze the suboptimal morphology that causes the bimolecular recombination.

2. EXPERIMENTAL SECTION

2.1. Nanoparticle Synthesis. Poly[[2,5-bis(2-hexyldecyl)-2,3,5,6-tetrahydro-3,6-dioxopyrrolo[3,4-*c*]pyrrole-1,4-diyl](3‴,4′-dihexyl-[2,2′:5′,2″:5″,2‴:5‴,2⁗-quinquethiophene]-5,5⁗-diyl)] (PDPP5T)[28] and [60]PCBM or [70]PCBM (Solenne BV) were dissolved in a 1:2 weight ratio in chloroform (30 mg in 0.75 mL) and stirred for 1 h at 90 °C. Solutions of SDS (Acros Organics) in ultrapure water were prepared separately at different concentrations. The chloroform solution was added to the aqueous SDS solution under vigorous stirring. The emulsion was then directly sonicated with a Sonics Vibracell VC 750 (Sonics & Materials Inc.) for 4 min at 30% amplitude. The resulting miniemulsion was stirred for 4 h at 60 °C in a round-bottom flask heated by an oil bath to evaporate chloroform. Excess SDS was removed by dialysis utilizing dialysis tubing (10 kDa, 10 mm flat width) (Sigma-Aldrich) and stirring overnight in 5 L of water. After overnight dialysis, the water was refreshed, and dialysis was continued until the desired conductivity was reached. To increase the concentration of the dispersion to 37.5 mg/mL, it was concentrated by centrifugal dialysis utilizing Amicon Ultra-4 Centrifugal Filters with a 10 kDa membrane (Milipore) at 2000 relative centrifugal force.

2.2. Solar Cell Fabrication. Photovoltaic devices were made by either spin coating a ZnO sol gel layer or ethoxylated-polyethyleni-

DOI: 10.1021/acsami.7b00557
ACS Appl. Mater. Interfaces 2017, 9, 13380−13389

mine (PEIE) layer on cleaned, patterned indium tin oxide (ITO) substrates in air (14 Ω per square) (Naranjo Substrates). The ZnO sol gel was prepared by dissolving $Zn(OAc)_2$ (Sigma-Aldrich) (109.6 mg) in 2-methoxyethanol (Sigma-Aldrich) (1 mL) and adding ethanolamine (Sigma-Aldrich) (30.2 μL). Then, the mixture was stirred at room temperature for at least 1 h. This sol gel was spin coated at 4000 rpm and annealed for 5 min at 150 °C under ambient conditions. PEIE dissolved in 2-propanol (2.24 mg/mL) was spin coated at 5000 rpm and annealed at 150 °C for 10 min. NPs were spin coated on top of the electron transporting layer and dried for 5 min at 110 °C. To wash off the surfactant, the devices were washed in a water/ethanol mixture (500 mL, 50:50 v/v) for 30 min under continuous stirring. Subsequently, the layers were dried for 5 min at 110 °C to remove the water, after which they were transferred to a glovebox, where they were annealed at 140 °C for 10 min. To make a BHJ, PDPP5T and [60]PCBM were dissolved in a 1:2 weight ratio in chloroform to a concentration of 18 mg/mL to which 4.8 vol % o-DCB was added. This solution was spin coated at 2000 rpm on a glass/ITO/PEIE substrate to obtain an active layer thickness of 100 nm. The devices were finished by evaporating MoO_3 (10 nm) and Ag (100 nm) as top electrode under a vacuum of $\sim 3 \times 10^{-7}$ mbar. The active area of the cells was 0.09 or 0.16 cm^2, which gave similar results.

2.3. Characterization. Dynamic light scattering (DLS) was measured with a Malvern Zetasizer μV on diluted samples (~0.09 mg/mL) at 25 °C. The laser wavelength was 830 nm, and measurements were performed in disposable, plastic, low-volume cuvettes. DLS measures the hydrodynamic diameter. For a non-spherical particle, DLS will give the diameter of a sphere that has the same average translational diffusion coefficient as the particle being measured. The mean particle size was calculated by integrating the intensity distribution, and the final result represents the average from five measurements. The standard deviation is about 4%. *Z*-average sizes were not used because not all dispersions showed a unimodal particle size distribution.

Conductivity and ζ-potential (ZP) were measured with a Malvern instruments Zetasizer Nano-ZS at 20 °C. To measure the conductivity of the dispersion during dialysis, the dispersion was removed from the dialysis tube, measured, and placed back in the same membrane to continue dialysis. For all devices prepared in this work (except where noted otherwise), the conductivity of the dispersions was measured. For ZP measurements, diluted dispersions were used with a concentration of 0.09 mg/mL. The laser wavelength was 633 nm, and measurements were performed in disposable folded cuvettes (Malvern Zetasizer Nano Series DTS1070).

Transmission electron microscopy (TEM) samples were prepared by floating of the active layer from a ZnO sol gel layer. The ZnO layer was dissolved in acidified water after which the active layer was transferred to a 200 square mesh copper grid. For analyzing the layers, a Tecnai G2 Sphere was used with a high tension of 200 kV at a magnification range of 1150× to 80 000× and corresponding defocus values of −10 μm and −400 nm, respectively. To avoid beam damage to the sample, the beam was blocked in low-dose mode while moving to another position at the sample. For cryo-TEM, dispersions with a concentration of 3 mg/mL were used and analyzed with a FEI Titan TEM. Samples were prepared by a Vitrobot, where 3 μL of the dispersion was placed on a 100 holey carbon coated 200 square mesh copper grid (Quantafoil, R2/2). Excess of sample was removed by blotting with a filter paper, and then the sample was frozen in liquid ethane. The samples were analyzed at a magnification range of 6500× to 61 000× with a defocus ranging from −20 μm to −250 nm, respectively.

Atomic force microscopy (AFM) was measured in tapping mode using a Veeco MultiMode. PPP-NCHR-50 tips were purchased from Nanosense.

Optical absorption was measured with a PekinElmer Lambda 900 UV/vis/near IR spectrophotometer. The absorption was measured on diluted dispersion and solution samples which had concentrations of 0.09 and 0.06 mg/mL, respectively. The spectra were measured with respect to a reference sample containing either water or a mixture of chloroform with 4.8 vol % *o*-DCB. Films were prepared by spin coating the solution and dispersion on a glass substrate containing an electron transporting layer. Optical modeling was performed within the transfer matrix formalism using the complex refractive index and the thicknesses of all materials in the layer stack as input. Calculations were performed with Setfos 4.3 (Fluxim, AG, Switzerland).

Current density−voltage (*J*−*V*) curves were measured under simulated solar light of 100 mW/cm^2. This was achieved by a Hoya LB100 daylight filter that was placed in between the solar cell and a tungsten−halogen lamp. To perform a *J*−*V* sweep, a Keithley 2400 sourcemeter was used. All measurements were conducted in a nitrogen-filled glovebox. Device performances are quoted as maximum power (P_{max}, mW/cm^2) when the short-circuit current density (J_{SC}) was obtained from the *J*−*V* curve measured under simulated solar light of 100 mW/cm^2 and as PCE (%) when J_{SC} was determined more accurately from the external quantum efficiency (EQE) by integrating the EQE with the AM1.5G solar spectrum.

EQE measurements were performed in a home-built setup which consists of a 50 W tungsten halogen lamp (Osram 64610), a mechanical chopper (Stanford Research Systems, SR 540), a monochromator (Oriel, Cornerstone 130) and finally the device kept in a nitrogen filled box with a quartz window which was illuminated through an aperture of 2 mm. This measurement was also performed in combination with a continuous LED bias light with a wavelength of 730 nm (Thorlabs). The current of this bias light can be adjusted such that an illumination intensity equal to AM1.5G is reached. The response was recorded using a low noise current preamplifier (Stanford Research Systems SR 570) and lock-in amplifier (Stanford Research Systems SR 830).

3. RESULTS AND DISCUSSION

3.1. Nanoparticle Synthesis. NPs were fabricated from a 1:2 blend of PDPP5T and [60]PCBM in chloroform using the miniemulsion method (Figure 1). The chloroform solution was introduced into water containing SDS and, after applying a high shear by sonication, a miniemulsion is formed. Subsequent evaporation of chloroform resulted in a stabilized dispersion of NPs in water. The initial concentration of SDS in the miniemulsion determines the NP size, which did not change during subsequent dialysis of the dispersion to remove excess SDS. High SDS concentrations gave smaller NPs than did low concentrations. By varying the SDS concentration ([SDS]) between 10.2 and 41.2 mM, a good control over the NP size could be obtained in range of 62−34 nm (Table 1, Figure 2).

Table 1. Nanoparticle Diameter Determined by DLS as Function of SDS Concentration

[SDS] (mM)	mean size (nm)
41.2	34
20.3	42
14.5	53
10.2	62

3.2. Optical Properties. The optical absorption maximum of PDPP5T exhibits a red shift from 680 to 708 nm when a chloroform solution of PDPP5T and [60]PCBM is introduced into the aqueous SDS solution and subsequently sonicated (Figure 3a). This red shift is characteristic for PDPP5T in an aggregated state and results from interchain interactions and planarization of the polymer chains.[7,29] An additional red shift of 16 nm is observed after removal of chloroform, indicating an enhanced aggregation. Dialysis of the dispersion has no further effect on the absorption spectrum. After dialysis, the dispersion can be concentrated, spin coated, and subsequently annealed at 140 °C for 10 min to form a thin film. The absorption spectrum

DOI: 10.1021/acsami.7b00557
ACS Appl. Mater. Interfaces 2017, 9, 13380−13389

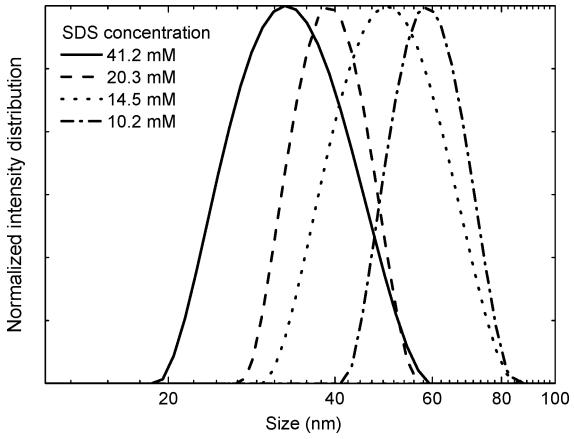

Figure 2. DLS measurements showing the effect of the SDS concentration on the size of PDPP5T:[60]PCBM nanoparticles.

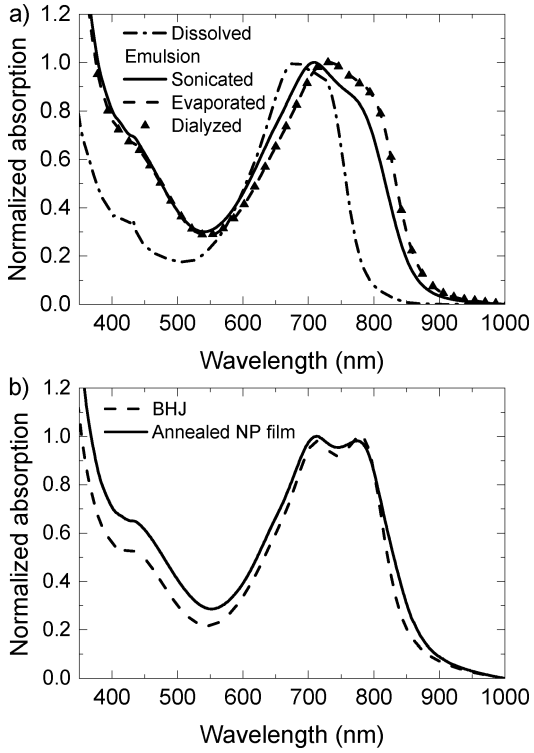

Figure 3. Optical absorption spectra of PDPP5T:[60]PCBM. (a) Solution and dispersion, recorded at various stages of the miniemulsion method. (b) Spin coated and annealed NP film and BHJ film processed from chloroform with 4.8 vol % *o*-DCB.

of this film is very similar to that of a BHJ layer processed from a chloroform:*o*-DCB, indicating comparable levels of aggregation of the polymer (Figure 3b). Because polymer aggregation is important for efficient charge transport, the similar aggregation after deposition by two different processing methods is an important observation.

3.3. Solar Cell Performance. After synthesizing the NPs the dispersion was concentrated by centrifugal dialysis until a concentration of 37.5 mg/mL. The NPs were then applied on a substrate (i.e., glass/ITO/ZnO or glass/ITO/PEIE) by spin coating. For NP devices processed on PEIE, an additional washing step was performed to remove excess surfactant from the active layer. It is known that during drying of the active layer, the NPs coalesce and exclude SDS to the film−air interface where they take a preferential orientation.[30,31] This was also observed for our layers, and AFM analysis showed that these surfactants can be efficiently washed off by dipping the substrates into a water/ethanol (50:50 v/v) mixture and subsequent drying at 110 °C (Supporting Information, Section 1). The water contact angle measured for annealed and washed NP layers was identical to that of the conventional BHJ blend processed from chloroform/o-DCB. Although we have no evidence of residual SDS in the films, its presence cannot be excluded. Washing in water/ethanol was not possible when ZnO was used as the electron transport layer because ZnO is not resistant to the washing step. NP devices were finished by evaporating a MoO_3/Ag top contact. In this section, we discuss relevant trends of the solar cell performance, their reproducibility, performance optimization, and current limitations. For comparison, a reference cell with a PCE of 5.8% ($J_{SC,EQE}$ = 16.6 mA/cm^2, V_{OC} = 0.58, FF = 0.60) was made by processing PDPP5T:[60]PCBM in a 1:2 ratio from chloroform containing 4.8 vol % *o*-DCB.

3.3.1. Effect of Annealing, Layer Thickness, and NP Size. NP devices processed on ZnO and dried at 110 °C under ambient conditions gave a low performance (Table 2).

Table 2. Effect of Annealing on Device Performance[a]

d (nm)	annealing (°C)	J_{SC} (mA/cm^2)	V_{OC} (V)	FF	P_{max} (mW/cm^2)
66	110	3.35	0.45	0.43	0.65
61	140	6.65	0.49	0.41	1.36

[a]ITO/ZnO/PDPP5T:[60]PCBM NPs/MoO_3/Ag configuration. NPs were synthesized with a 41.2 mM starting concentration of SDS. The conductivity of the dispersions used to make these devices was not measured.

Annealing under nitrogen for 10 min at 140 °C significantly improved the device performance (Table 2), consistent with previous results.[21,32,33] Similar device performance was obtained for layers processed on PEIE as the electron transport layer (Supporting Information, Section 2). Processing of the NP layers on ZnO has the advantage that the layer can be analyzed by TEM because the ZnO layer dissolves in acidic water such that the NP layer floats on the water surface. This is not possible when PEIE is used. After drying of the NP layer, separate NPs can be distinguished in TEM (Figure 4a). However, annealing at 140 °C causes the NPs to coalesce into a continuous film, and its morphology starts to approach that of a BHJ spin coated from chloroform:*o*-DCB mixture (Figures 4b and c). Despite the positive effect of annealing at 140 °C on the performance of NP solar cells, a negative effect of annealing on the performance was found for chloroform:*o*-DCB processed

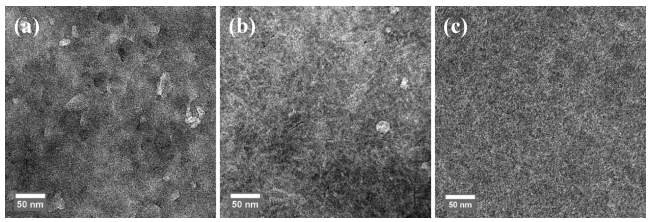

Figure 4. TEM images of PDPP5T:[60]PCBM blends at 50 000× and a defocus value of −1 μm. (a) NP layer after drying for 5 min at 110 °C. (b) NP layer after drying and annealing for 10 min at 140 °C. (c) BHJ processed from chloroform with 4.8 vol % *o*-DCB.

DOI: 10.1021/acsami.7b00557
ACS Appl. Mater. Interfaces 2017, 9, 13380−13389

BHJs (Supporting Information, Section 3). Therefore, thermal annealing may be limiting the performance of NP devices.

Further optimization was performed on ITO/PEIE/PDPP5T:[60]PCBM NPs/MoO_3/Ag devices because of their higher reproducibility of devices on PEIE compared to that on ZnO. Optimization of the layer thickness (d) revealed that the best performance was obtained at $d \approx 70$ nm (Table 3), which is thinner than the optimum of $d \approx 100$ nm for conventional BHJs cells. With increasing layer thickness, J_{SC} increases while the FF decreases, and V_{OC} does not change significantly (Table 3). Such trend is frequently observed in organic solar cells and originates from a competition between increased light absorption, resulting in more charges and stronger bimolecular charge recombination for thicker layers. The effect of increasing J_{SC} with increasing layer thickness up to 68 nm is caused by a significant increase of light absorption by the polymer, contributing to the generated current as evidenced by the EQE spectra (Figure 5a). The EQE spectra also show that with increasing thickness the contribution of [60]PCBM in the UV region decreases with a concomitant shift of the [60]PCBM band to higher wavelengths. By modeling the absorption spectra using the refractive index (n) and extinction coefficient (k) of the blend (Supporting Information, Section 4) in the layer stack, it was found that this shift is reproduced in the simulations and is due to the interference of light (Figure 5b). The decrease of this EQE band, however, is not reproduced in the modeled spectra and indicates that the contribution of absorption of light by [60]PCBM to the photocurrent becomes less for thicker layers. For the polymer absorption between 550 and 850 nm, on the other hand, the increase in EQE for thicker layers matches with the increased absorption of light. Eventually, a small drop in EQE occurred when increasing the thickness to 93 nm, which is likely related to the very low FF of this device. Compared to the normal BHJ, where FF = 0.6 at $d = 100$ nm, the FF for the NP devices is rather low. This suggests increased bimolecular charge recombination, which will be addressed in Section 3.3.3. More details about the device statistics can be found in the Supporting Information (Section 5).

Table 3. Performance of PDPP5T:[60]PCBM NP Cells for Different Active Layer Thickness[a]

d (nm)	J_{SC} (mA/cm^2)	V_{OC} (V)	FF	P_{max} (mW/cm^2)
47	4.88	0.53	0.55	1.41
51	5.38	0.55	0.53	1.57
60	6.48	0.53	0.49	1.71
68	7.03	0.55	0.44	1.73
93	6.60	0.50	0.38	1.28

[a]NPs synthesized with a 20.3 mM starting SDS concentration. Different active layer thickness achieved by varying spin speed between 800−2400 rpm.

The effect of NP size on device performance was studied using different NP dispersions. Table 4 shows the average device performance for four NP sizes when the active layer thickness was optimized by adjusting the spin speed and using a constant NP of 37.5 mg/mL. In general, J_{SC} and PCE decrease with increasing NP size. A possible explanation might be a decrease in D/A interface in active layers processed from larger particles. No clear trend in FF with NP size is observed because the FF is dominated by the layer thickness.

Table 4. Effect of NP Size on the Device Performance

particle size (nm)[a]	d (nm)	J_{SC} (mA/cm^2)	V_{OC} (V)	FF	P_{max} (mW/cm^2)
32	59	6.52	0.54	0.48	1.70
44	68	7.03	0.55	0.44	1.73
54	46	5.05	0.50	0.48	1.21
60	71	4.88	0.49	0.44	1.05

[a]The size of the particles was measured after $CHCl_3$ evaporation.

3.3.2. Reproducibility: Conductivity and ζ-Potential Measurements. Despite the successful fabrication of solar cells from aqueous miniemulsions, the reproducibility is not optimal. As an example, the second entry of Table 2 and the first entry of Table 4 are nominally almost the same cells but differ in P_{max} (1.36 vs 1.70 mW/cm^2). This variability is caused by fluctuations in the SDS concentration in the final dispersion between different runs. The rate of SDS removal during dialysis is highly sensitive to stirring speed, the shape of the dialysis container, the amount of water, and the surfactant concentration in the dispersion and water phase. To monitor SDS concentration in the dispersion during dialysis, conductivity (κ) and ζ-potential measurements were performed. The conductivity is a measure for the amount of free surfactant, while the ζ-potential measures the surface charge and reflects the amount of surfactant bound to the surface of the particle. The ζ-potential gives valuable information about the stability of the dispersion obtained by electrostatic forces between particles. Figure 6a shows that during overnight dialysis the conductivity

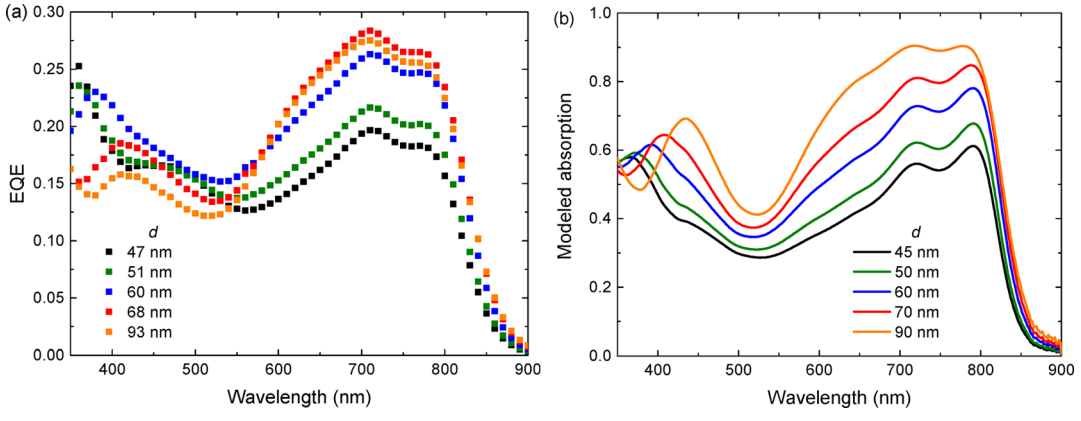

Figure 5. Effect of the thickness of PDPP5T:[60]PCBM layers on (a) EQE and (b) the modeled absorption spectra.

DOI: 10.1021/acsami.7b00557
ACS Appl. Mater. Interfaces 2017, 9, 13380−13389

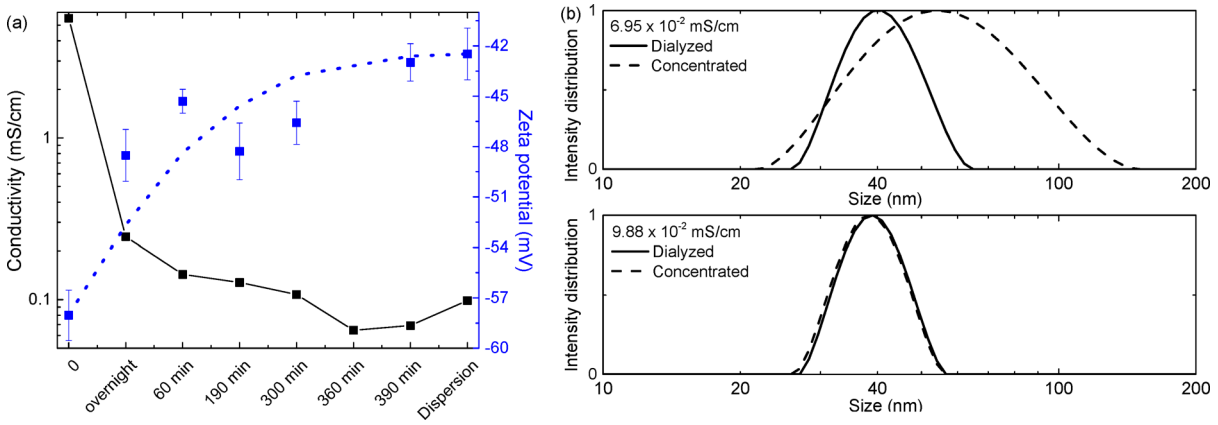

Figure 6. (a) Conductivity and ζ-potential of a dispersion during dialysis. The final point called "dispersion" resembles the conductivity of the concentrated dispersion. (b) Effect of the final conductivity of the dispersion on the size of the NPs with low (upper graph) and high (lower graph) conductivity.

steeply decreases. After the water is refreshed, the conductivity decreases further, and the time of dialysis is critical to the final SDS concentration. Because the SDS in the solution is in equilibrium with SDS adsorbed to the particles,[34] the ζ-potential increases toward less negative surface charge during the dialysis. This results in less stable dispersions and ultimately aggregation, especially after concentrating. Figure 6b shows that the particle size increased after concentrating a dispersion with a low SDS concentration, while no aggregation occurred when the SDS concentration was higher.

The SDS concentration also dramatically affects quality of the spin coated layers. When the SDS concentration is too high, holes are formed because of dewetting (Figure 7), but when the

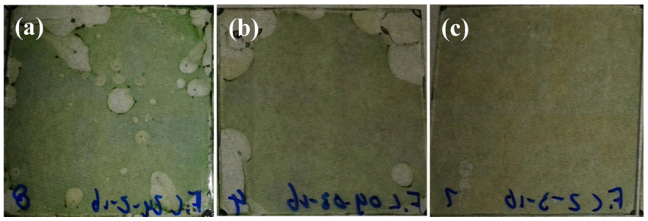

Figure 7. Images of the spin coated active layers from dispersions with decreasing conductivity: (a) $\kappa = 1.47 \times 10^{-1}$ mS/cm. (b) $\kappa = 7.19 \times 10^{-2}$ mS/cm. (c) $\kappa = 6.95 \times 10^{-2}$ mS/cm.

SDS concentration is too low, electrical shorts are formed because aggregation of NPs under these conditions creates rough active layers with pin holes (Supporting Information, Section 6). Only when a balance between the two is achieved by controlling the surfactant concentration can reproducible solar cell performance be obtained. Table 5 shows the relation between the conductivity (related to [SDS]) and the device performance. Further details about the statistics can be found in Section 7 of the Supporting Information. For 42 nm sized NPs (Table 1), the optimal balance between dewetting and aggregation occurs at a conductivity of 9.88×10^{-2} mS/cm. For smaller NPs of 34 nm, a higher optimal conductivity ($\sim 1.9 \times 10^{-1}$ mS/cm) was required because the concentration of free surfactants scales with the increased total surface area (Supporting Information, Section 8). We conclude that conductivity and ζ-potential tracking during dialysis are effective to monitor the free and bound SDS concentrations, thereby avoiding dewetting and aggregation. However, it must

Table 5. Performance of Solar Cells from Dispersions with Different Conductivity Levels[a]

κ (mS/cm)	aggregation	J_{SC} (mA/cm^2)	V_{OC} (V)	FF	P_{max} (mW/cm^2)
6.95×10^{-2}	yes	4.09	0.50	0.43	0.88
7.19×10^{-2}	slightly	5.63	0.50	0.48	1.33
9.88×10^{-2}	no	5.62	0.53	0.51	1.55
1.28×10^{-1}	no	shorted			
1.47×10^{-1}	no	shorted			
2.06×10^{-1}	no	shorted			

[a]NPs were synthesized with a 20.3 mM starting SDS concentration.

be noted that the solar cell performance is sensitive to small deviations from optimal conductivity, requiring careful tracking of the dialysis speed.

3.3.3. Improving Solar Cell Performance. When [60]PCBM is replaced by [70]PCBM as electron acceptor in the NPs, the optical absorption in the range of 400−600 nm increased (Supporting Information, Section 9). As a result, the short-circuit current density significantly improved, resulting in a maximum PCE of 2.36% for PDPP5T:[70]PCBM NP cells (Table 6 and Supporting Information, Section 10) when using procedures for preparation and dialysis of the NPs the same as those for PDPP5T:[60]PCBM. This level of performance is comparable to optimized NP solar cells from other materials.[22,23,25,33,35−37] For the NP cells with [70]PCBM as acceptor, we found a similar trade-off between an increasing J_{SC} and decreasing FF for thicker films (Table 6) as that found for [60]PCBM (Table 3). The reduction in FF for thicker layers is attributed to increased bimolecular recombination. This can be seen by measuring the EQE with and without bias light (Figure 8) because the ratio of the EQE measured under AM1.5G equivalent bias light and the EQE measured under low light intensity, $\rho = EQE_{bias}/EQE_{no\ bias}$ (integrated over the AM1.5 G spectrum), deceases when bimolecular recombination increases.[38] Table 6 reveals that ρ and concomitantly FF, decrease with increasing thickness (Table 6).

It has been reported that the efficiency of aqueous NP solar cells can be enhanced by the addition of 20 vol % ethanol to the dispersion.[35,37,39] Our results confirm this for PDPP5T:[60]PCBM NP devices (Table 7). Addition of ethanol improves the J_{SC} and PCE. To avoid aggregation of the NPs, ethanol has to be added carefully. To this end, we first

DOI: 10.1021/acsami.7b00557
ACS Appl. Mater. Interfaces 2017, 9, 13380−13389

Table 6. Performance of PDPP5T:[70]PCBM NP Cells for Different Active Layer Thickness[a]

d (nm)	J_{SC} (mA/cm^2)	$J_{SC,\ EQE}$ (mA/cm^2)	V_{OC} (V)	FF	P_{max} (mW/cm^2)	PCE (%)	ρ
67	10.70	9.84	0.53	0.42	2.35	2.31	0.82
50	9.34	9.15	0.54	0.47	2.38	2.36	0.89
36	6.70	7.00	0.51	0.50	1.69	1.77	0.94

[a]NPs were synthesized with a 41.2 mM starting SDS concentration.

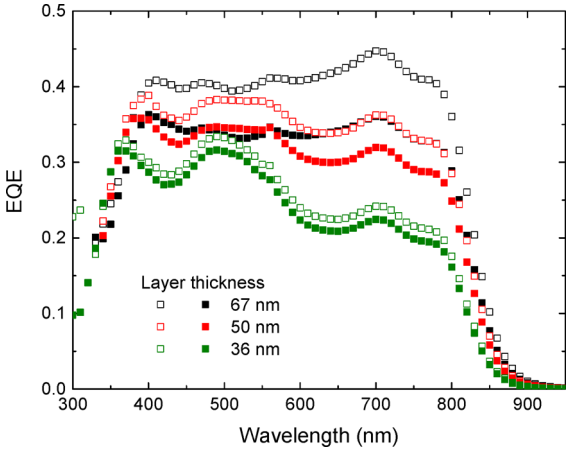

Figure 8. EQE of PDPP5T:[70]PCBM NP solar cells without (open symbols) and with (solid symbols) light bias (730 nm) for three different active layer thicknesses.

Table 7. Effect of Adding Ethanol to the Dispersion on the Device Performance[a]

d (nm)	ethanol (vol %)	J_{SC}, EQE (mA/cm2)	V_{OC} (V)	FF	PCE (%)
62	0	4.54	0.57	0.50	1.30
63	20	6.58	0.56	0.54	1.99

[a]NPs were synthesized with a 20.3 mM starting SDS concentration.

concentrated the dispersion to ~75 mg/mL and then slowly added ethanol in water to reach 37.5 mg/mL with 20 vol % ethanol.

Interestingly, also aging of the PDPP5T:[60]PCBM NP dispersions is beneficial for the device performance. Solar cells fabricated over a period of 10 days from a single batch of 44 nm sized NPs (Table 8 and Supporting Information, Section 11)

Table 8. Effect of Aging on Solar Cell Performance for 44 nm NP Dispersions

day	d (nm)	J_{SC} (mA/cm^2)	V_{OC} (V)	FF	P_{max} (mW/cm^2)
0[a]	75	6.72	0.51	0.45	1.54
1	85	9.20	0.48	0.43	1.93
2	81	8.32	0.53	0.47	2.04
5	86	8.31	0.51	0.44	1.89
9	80	8.00	0.50	0.46	1.85

[a]Day 0 corresponds to the day at which the dialysis was performed and the dispersion was concentrated.

show improved performance with time due to a significant increase in J_{SC} (Table 8) and EQE (Figure 9) after the first day. The best device was made after 1 day of aging with a PCE of 2.03% ($J_{SC,\ EQE}$ = 9.07 mA/cm^2, V_{OC} = 0.51 V, FF = 0.44, see Supporting Information, Section 12). After two days, similar efficiencies were obtained. On prolonged aging, the average performance dropped slightly, caused by a slowly decreasing

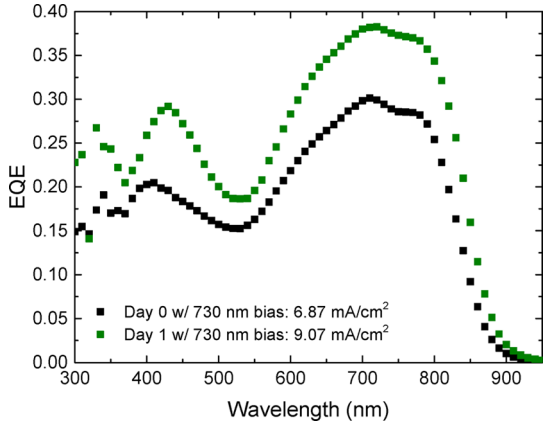

Figure 9. EQE spectra of the best PDPP5T:[60]PCBM NP devices fabricated from a dispersion without aging (black symbols) and after one day of aging (green symbols).

J_{SC}, but the changes with time are close to the experimental error.

A similar positive effect of one-day aging, although less pronounced, has been observed for a 31 nm sized NP dispersion, which is illustrated in the Supporting Information (Section 13).

ζ-potential measurements were performed to find the cause for this beneficial aging effect. For the 44 nm sized NPs, the surface charge decreases from −39 ± 1.8 mV at day 0 to −30 ± 2.1 mV at day 1. During further storage, the ζ-potential remains within experimental error. Apparently, a stabilization time is necessary after concentrating the dispersion to restore the balance between free and bound surfactants. It is known that ionic stabilization of particles can hamper the film formation.[30,31] When an aqueous dispersion is spin coated on a substrate, the film formation process consists out of several steps: (i) water evaporation, (ii) packing of NPs, (iii) deformation, and finally (iv) coalescence into a homogeneous film. Surfactant molecules stabilizing the NP dispersion can negatively influence the coalescence due to electrostatic repulsion. We think that the reduction in ζ-potential promotes the coalescence and the formation of the particles into a continuous film. The enhanced film formation after aging improves charge transport and increases J_{SC}.

A similar mechanism resulting in improved film formation may also be responsible for the improved performance when ethanol is added to the dispersion (Table 7) because ethanol can influence the balance between surface-bound and free surfactant. Both methods gave similar PCEs up to 2%. Because aging is a more gentle method and, unlike adding of ethanol, does not cause aggregation of the particles (Supporting Information, Section 14), aging improves both performance and reproducibility.

3.4. Morphology Studied by Cryo-TEM. In this study, a maximum PCE of 2.03% with [60]PCBM and 2.36% with [70]PCBM was achieved for NP solar cells based on PDPP5T.

DOI: 10.1021/acsami.7b00557
ACS Appl. Mater. Interfaces 2017, 9, 13380−13389

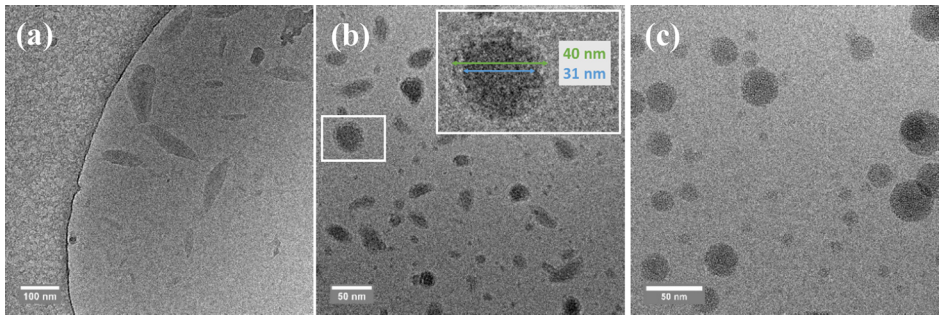

Figure 10. Cryo-TEM of aqueous NP dispersions after evaporation of chloroform. (a) PDPP5T (24 000× , −5 μm defocus). (b) PDPP5T:[60]PCBM in a 1:2 weight ratio (48 000× , −2.5 μm defocus). The inset shows magnification of a single particle which indicates the core and shell. (c) [60]PCBM (61 000× , −250 nm defocus).

The performance is less than that of conventional BHJ cells and likely limited by a nonoptimized morphology. The morphology of the active layer is in these NP systems is determined by the degree of mixing between the two compounds in a single NP. Cryo-TEM was performed to visualize the NPs in the aqueous dispersion (Figure 10). NPs made from PDPP5T appear elongated, while particles made from [60]PCBM are spherical. This difference in shape is likely related to the semicrystalline nature of PDPP5T. Nonspherical nanoparticles in aqueous miniemulsions have previously been observed for liquid-crystalline and crystalline polymers.[33,40−42] The shape anisotropy is attributed to the underlying order of the polymer chains in the nanoparticle.[40] When combining the two materials in one particle, the NP shape is prolate (elongated) spheroid. The particle size observed by TEM corresponds to the one measured by DLS. Interestingly, the particles have a dark core surrounded by a light colored shell (inset of Figure 10b), which can be due to phase separation within the particle. On the basis of contrast differences in the cryo-TEM measurements, a shell thickness between 3−6 nm was estimated. Contrast differences in bright-field TEM can be caused by thickness and compositional variations. For the pure PDPP5T and pure [60]PCBM particles, there is no strong contrast change toward the outside of the particles. Hence, the nonuniform contrast of the mixed particles can be interpreted as a core−shell morphology. The surface tensions (γ) of PDPP5T (20.2 mN/m) and [60]PCBM (35.4 mN/m), as determined from contact angle measurements using Neumann's method, differ considerably. Because of its lower surface tension, PDPP5T is expected on the outside, and [60]PCBM is expected on the inside. The phase separation during drying of these two compounds in a chloroform solution has shown that the PDPP5T and [60]PCBM are incompatible due to a high Flory−Huggins interaction parameter.[43] A core−shell morphology of NPs in aqueous dispersions was also observed for other material combinations having similar differences in surface tension.[20,22,23,36,44,45] In our view, such core−shell morphology limits the performance of the NP solar cells.

4. CONCLUSIONS

We investigated solar cells based on PDPP5T and [60]PCBM processed from aqueous nanoparticle dispersions. The size of the mixed PDPP5T:[60]PCBM nanoparticles can be controlled by varying the surfactant (SDS) concentration at the start of the process. The SDS concentration in the NP dispersion used for preparing the photovoltaic layers is important in the film forming process. A too-high SDS concentration causes dewetting, while a too-low concentration results in aggregation of the NPs. Both give rise to shorted devices and limit the reproducibility of the device performance. By controlling the amount of free and surface-bound SDS via measuring the conductivity and ζ-potential of the dispersions, solar cells can be made reproducibly.

We further showed that (i) replacing [60]PCBM by [70]PCBM to increase light absorption, (ii) addition of ethanol to the dispersion, or (iii) aging the dispersion for one day results in improved performance. Aging for one day results in a reduction of the surface charge of the NPs and improves film formation. Optimized NP cells based on PDPP5T with [60]PCBM and [70]PCBM gave power conversion efficiencies of 2.0 and 2.4%, respectively.

The PCEs of the PDPP5T:PCBM NP solar cells still fall short compared to those of optimized bulk heterojunction solar cells. This is caused by nonoptimized morphology, which results in more pronounced bimolecular recombination, reducing the FF and limiting the optimal thickness of the photoactive layer to a range where a too-small fraction of light is absorbed and thereby reducing the short-circuit current density (J_{SC}). Cryo-TEM suggest that the NPs possess a core−shell-like morphology with PDPP5T dominating in the shell of the particle and PCBM in the center. This hampers electron collection and thereby enhances bimolecular recombination. Further research can focus on exploring how such core−shell morphology can be prevented and if this improves device performance.

■ ASSOCIATED CONTENT

Supporting Information

The Supporting Information is available free of charge on the ACS Publications website at DOI: 10.1021/acsami.7b00557.

Further experimental results on morphology and device performance under different processing conditions (PDF)

■ AUTHOR INFORMATION

Corresponding Author

*E-mail: r.a.j.janssen@tue.nl.

ORCID

René A. J. Janssen: 0000-0002-1920-5124

Notes

The authors declare no competing financial interest.

DOI: 10.1021/acsami.7b00557
ACS Appl. Mater. Interfaces 2017, 9, 13380−13389

■ ACKNOWLEDGMENTS

We would like to thank Paul Bomans and Anne Spoelstra for the cryo-TEM measurements and their help with analyzing films by TEM. This research is supported by the Dutch Technology Foundation STW, which is part of The Netherlands Organisation for Scientific Research (NWO) and which is partly funded by the Ministry of Economic Affairs (Project 13513). The research leading to these results also received funding from the European Research Council under the European Union's Seventh Framework Programme (FP/2007-2013)/ERC Grant Agreement 339031) and from the Ministry of Education, Culture and Science (Gravity Program 024.001.035).

■ REFERENCES

(1) Wang, Q.; Xie, Y.; Soltani-Kordshuli, F.; Eslamian, M. Progress in Emerging Solution-Processed Thin Film Solar Cells − Part I: Polymer Solar Cells. *Renewable Sustainable Energy Rev.* **2016**, *56*, 347−361.

(2) Søndergaard, R.; Hösel, M.; Angmo, D.; Larsen-Olsen, T. T.; Krebs, F. C. Roll-to-Roll Fabrication of Polymer Solar Cells. *Mater. Today* **2012**, *15* (1−2), 36−49.

(3) Jao, M.-H.; Liao, H.-C.; Su, W.-F. Achieving a High Fill Factor for Organic Solar Cells. *J. Mater. Chem. A* **2016**, *4* (16), 5784−5801.

(4) Ding, Z.; Stoichkov, V.; Horie, M.; Brousseau, E.; Kettle, J. Spray Coated Silver Nanowires as Transparent Electrodes in OPVs for Building Integrated Photovoltaics Applications. *Sol. Energy Mater. Sol. Cells* **2016**, *157*, 305−311.

(5) Chai, Z.; Zhang, N.; Sun, P.; Huang, Y.; Zhao, C.; Fan, H. J.; Fan, X.; Mai, W. Tailorable and Wearable Textile Devices for Solar Energy Harvesting and Simultaneous Storage. *ACS Nano* **2016**, *10* (10), 9201−9207.

(6) Kawashima, K.; Tamai, Y.; Ohkita, H.; Osaka, I.; Takimiya, K. High-Efficiency Polymer Solar Cells with Small Photon Energy Loss. *Nat. Commun.* **2015**, *6*, 10085−10093.

(7) Li, W.; Roelofs, W. S. C.; Wienk, M. M.; Janssen, R. A. J. Enhancing the Photocurrent in Diketopyrrolopyrrole-Based Polymer Solar Cells via Energy Level Control. *J. Am. Chem. Soc.* **2012**, *134* (33), 13787−13795.

(8) Zhang, F.; Inganäs, O.; Zhou, Y.; Vandewal, K. Development of Polymer−fullerene Solar Cells. *Natl. Sci. Rev.* **2016**, *3* (2), 222−239.

(9) Van Franeker, J. J.; Heintges, G. H. L.; Schaefer, C.; Portale, G.; Li, W.; Wienk, M. M.; van der Schoot, P.; Janssen, R. A. J. Polymer Solar Cells: Solubility Controls Fiber Network Formation. *J. Am. Chem. Soc.* **2015**, *137* (36), 11783−11794.

(10) Zhao, J.; Li, Y.; Yang, G.; Jiang, K.; Lin, H.; Ade, H.; Ma, W.; Yan, H. Efficient Organic Solar Cells Processed from Hydrocarbon Solvents. *Nat. Energy* **2016**, *1* (2), 15027−15033.

(11) Wan, Q.; Guo, X.; Wang, Z.; Li, W.; Guo, B.; Ma, W.; Zhang, M.; Li, Y. 10.8% Efficiency Polymer Solar Cells Based on PTB7-Th and $PC_{71}BM$ via Binary Solvent Additives Treatment. *Adv. Funct. Mater.* **2016**, *26* (36), 6635−6640.

(12) Liu, Y.; Zhao, J.; Li, Z.; Mu, C.; Ma, W.; Hu, H.; Jiang, K.; Lin, H.; Ade, H.; Yan, H. Aggregation and Morphology Control Enables Multiple Cases of High-Efficiency Polymer Solar Cells. *Nat. Commun.* **2014**, *5* (9), 6293−6300.

(13) Zang, Y.; Gao, X.; Lu, X.; Xin, Q.; Lin, J.; Zhao, J. Improved Performance of Polymer Solar Cells Using PBDTT-F-TT:PC71BM Blend Film as Active Layer. *Appl. Surf. Sci.* **2016**, *376*, 138−144.

(14) Zhang, J.; Zhang, Y.; Fang, J.; Lu, K.; Wang, Z.; Ma, W.; Wei, Z. Conjugated Polymer-Small Molecule Alloy Leads to High Efficient Ternary Organic Solar Cells. *J. Am. Chem. Soc.* **2015**, *137* (25), 8176−8183.

(15) Office of Environment and Heritage NSW. *Management of Chlorinated Solvents: Strategic Environmental Compliance and Performance Review*; New South Wales Office of Environment and Heritage: Sydney, 2011.

(16) Zhang, S.; Ye, L.; Zhang, H.; Hou, J. Green-Solvent-Processable Organic Solar Cells. *Mater. Today* **2016**, *19* (9), 533−543.

(17) Gärtner, S.; Christmann, M.; Sankaran, S.; Röhm, H.; Prinz, E.-M.; Penth, F.; Pütz, A.; Türeli, A. E.; Penth, B.; Baumstümmler, B.; Colsmann, A. Eco-Friendly Fabrication of 4% Efficient Organic Solar Cells from Surfactant-Free P3HT:ICBA Nanoparticle Dispersions. *Adv. Mater.* **2014**, *26* (38), 6653−6657.

(18) Sankaran, S.; Glaser, K.; Gärtner, S.; Rödlmeier, T.; Sudau, K.; Hernandez-Sosa, G.; Colsmann, A. Fabrication of Polymer Solar Cells from Organic Nanoparticle Dispersions by Doctor Blading or Ink-Jet Printing. *Org. Electron.* **2016**, *28*, 118−122.

(19) Landfester, K. Synthesis of Colloidal Particles in Miniemulsions. *Annu. Rev. Mater. Res.* **2006**, *36* (1), 231−279.

(20) Ulum, S.; Holmes, N.; Darwis, D.; Burke, K.; David Kilcoyne, a. L.; Zhou, X.; Belcher, W.; Dastoor, P. Determining the Structural Motif of P3HT:PCBM Nanoparticulate Organic Photovoltaic Devices. *Sol. Energy Mater. Sol. Cells* **2013**, *110*, 43−48.

(21) Holmes, N. P.; Nicolaidis, N.; Feron, K.; Barr, M.; Burke, K. B.; Al-Mudhaffer, M.; Sista, P.; Kilcoyne, a. L. D.; Stefan, M. C.; Zhou, X.; Dastoor, P. C.; Belcher, W. J. Probing the Origin of Photocurrent in Nanoparticulate Organic Photovoltaics. *Sol. Energy Mater. Sol. Cells* **2015**, *140*, 412−421.

(22) Dam, H. F.; Holmes, N. P.; Andersen, T. R.; Larsen-Olsen, T. T.; Barr, M.; Kilcoyne, a. L. D.; Zhou, X.; Dastoor, P. C.; Krebs, F. C.; Belcher, W. J. The Effect of Mesomorphology upon the Performance of Nanoparticulate Organic Photovoltaic Devices. *Sol. Energy Mater. Sol. Cells* **2015**, *138*, 102−108.

(23) Holmes, N. P.; Marks, M.; Kumar, P.; Kroon, R.; Barr, M. G.; Nicolaidis, N.; Feron, K.; Pivrikas, A.; Fahy, A.; Mendaza, A. D. D. Z.; Kilcoyne, A. L. D.; Müller, C.; Zhou, X.; Andersson, M. R.; Dastoor, P. C.; Belcher, W. J. Nano-Pathways: Bridging the Divide between Water-Processable Nanoparticulate and Bulk Heterojunction Organic Photovoltaics. *Nano Energy* **2016**, *19*, 495−510.

(24) Zhao, J.; Swinnen, A.; Van Assche, G.; Manca, J.; Vanderzande, D.; Mele, B. Van. Phase Diagram of P3HT/PCBM Blends and Its Implication for the Stability of Morphology. *J. Phys. Chem. B* **2009**, *113* (6), 1587−1591.

(25) D'Olieslaeger, L.; Pfannmöller, M.; Fron, E.; Cardinaletti, I.; Van Der Auweraer, M.; Van Tendeloo, G.; Bals, S.; Maes, W.; Vanderzande, D.; Manca, J.; Ethirajan, A. Tuning of PCDTBT:PC71BM Blend Nanoparticles for Eco-Friendly Processing of Polymer Solar Cells. *Sol. Energy Mater. Sol. Cells* **2017**, *159*, 179−188.

(26) D'Olieslaeger, L.; Pirotte, G.; Cardinaletti, I.; D'Haen, J.; Manca, J.; Vanderzande, D.; Maes, W.; Ethirajan, A. Eco-Friendly Fabrication of PBDTTPD:PC71BM Solar Cells Reaching a PCE of 3.8% Using Water-Based Nanoparticle Dispersions. *Org. Electron.* **2017**, *42*, 42−46.

(27) Van Franeker, J. J.; Turbiez, M.; Li, W.; Wienk, M. M.; Janssen, R. a J. A Real-Time Study of the Benefits of Co-Solvents in Polymer Solar Cell Processing. *Nat. Commun.* **2015**, *6*, 6229−6237.

(28) Hayoz, P.; Düggeli, M.; Chebotareva, N. O. F. A. Diketopyrrolopyrrole Polymers for Use in Organic Semiconductor Devices. WO 2011/144566A2, 2011.

(29) Mishra, A.; Schulz, G. L.; Kar, P.; Weidelener, M.; Vogt, A.; Urdanpilleta, M.; Linden, M.; Mena-Osteritz, E.; Baeuerle, P. The Influence of Alkyl Side Chains on Molecular Packing and Solar Cell Performance of Dithienopyrrole-Based Oligothiophenes. *J. Mater. Chem. A* **2016**, *4*, 10514−10523.

(30) Scalarone, D.; Lazzari, M.; Castelvetro, V.; Chiantore, O. Surface Monitoring of Surfactant Phase Separation and Stability in Waterborne Acrylic Coatings. *Chem. Mater.* **2007**, *19* (25), 6107−6113.

(31) Arnold, C.; Thalmann, F.; Marques, C.; Marie, P.; Holl, Y. Surfactant Distribution in Waterborne Acrylic Films. 1. Bulk Investigation. *J. Phys. Chem. B* **2010**, *114* (28), 9135−9147.

(32) Vaughan, B.; Stapleton, A.; Sesa, E.; Holmes, N. P.; Zhou, X.; Dastoor, P. C.; Belcher, W. J. Engineering Vertical Morphology with Nanoparticulate Organic Photovoltaic Devices. *Org. Electron.* **2016**, *32*, 250−257.

DOI: 10.1021/acsami.7b00557
ACS Appl. Mater. Interfaces 2017, 9, 13380−13389

(33) Vaughan, B.; Williams, E. L.; Holmes, N. P.; Sonar, P.; Dodabalapur, A.; Dastoor, P. C.; Belcher, W. J. Water-Based Nanoparticulate Solar Cells Using a Diketopyrrolopyrrole Donor Polymer. *Phys. Chem. Chem. Phys.* **2014**, *16* (6), 2647−2653.
(34) Li, Z.; Fichthorn, K. A.; Milner, S. T. Surfactant Binding to Polymer-Water Interfaces in Atomistic Simulations. *Langmuir* **2016**, *32* (30), 7519−7529.
(35) Gehan, T. S.; Bag, M.; Renna, L. a; Shen, X.; Algaier, D. D.; Lahti, P. M.; Russell, T. P.; Venkataraman, D. Multiscale Active Layer Morphologies for Organic Photovoltaics Through Self-Assembly of Nanospheres. *Nano Lett.* **2014**, *14* (9), 5238−5243.
(36) Ulum, S.; Holmes, N.; Barr, M.; Kilcoyne, A. L. D.; Gong, B.; Zhou, X.; Belcher, W.; Dastoor, P. The Role of Miscibility in Polymer:fullerene Nanoparticulate Organic Photovoltaic Devices. *Nano Energy* **2013**, *2* (5), 897−905.
(37) Yamamoto, N. A. D.; Payne, M. E.; Koehler, M.; Facchetti, A.; Roman, L. S.; Arias, A. C. Charge Transport Model for Photovoltaic Devices Based on Printed Polymer: Fullerene Nanoparticles. *Sol. Energy Mater. Sol. Cells* **2015**, *141*, 171−177.
(38) Koster, L. J. A.; Kemerink, M.; Wienk, M. M.; Maturová, K.; Janssen, R. A. J. Quantifying Bimolecular Recombination Losses in Organic Bulk Heterojunction Solar Cells. *Adv. Mater.* **2011**, *23*, 1670−1674.
(39) Bag, M.; Gehan, T. S.; Renna, L. a.; Algaier, D. D.; Lahti, P. M.; Venkataraman, D. Fabrication Conditions for Efficient Organic Photovoltaic Cells from Aqueous Dispersions of Nanoparticles. *RSC Adv.* **2014**, *4* (85), 45325−45331.
(40) Yang, Z.; Huck, W. T. S.; Clarke, S. M.; Tajbakhsh, A. R.; Terentjev, E. M. Shape-Memory Nanoparticles from Inherently Non-Spherical Polymer Colloids. *Nat. Mater.* **2005**, *4*, 486−490.
(41) Haseloh, S.; Ohm, C.; Smallwood, F.; Zentel, R. Nanosized Shape-Changing Colloids from Liquid Crystalline Elastomers. *Macromol. Rapid Commun.* **2011**, *32*, 88−93.
(42) Staff, R. H.; Lieberwirth, I.; Landfester, K.; Crespy, D. Preparation and Characterization of Anisotropic Submicron Particles from Semicrystalline Polymers. *Macromol. Chem. Phys.* **2012**, *213*, 351−358.
(43) Kouijzer, S.; Michels, J. J.; van den Berg, M.; Gevaerts, V. S.; Turbiez, M.; Wienk, M. M.; Janssen, R. a J. Predicting Morphologies of Solution Processed Polymer:fullerene Blends. *J. Am. Chem. Soc.* **2013**, *135* (32), 12057−12067.
(44) Schwarz, K. N.; Farley, S. B.; Smith, T. a; Ghiggino, K. P. Charge Generation and Morphology in P3HT: PCBM Nanoparticles Prepared by Mini-Emulsion and Reprecipitation Methods. *Nanoscale* **2015**, *7*, 19899−19904.
(45) Stapleton, A.; Vaughan, B.; Xue, B.; Sesa, E.; Burke, K.; Zhou, X.; Bryant, G.; Werzer, O.; Nelson, A.; David Kilcoyne, a. L.; Thomsen, L.; Wanless, E.; Belcher, W.; Dastoor, P. A Multilayered Approach to Polyfluorene Water-Based Organic Photovoltaics. *Sol. Energy Mater. Sol. Cells* **2012**, *102*, 114−124.

DOI: 10.1021/acsami.7b00557
ACS Appl. Mater. Interfaces 2017, 9, 13380−13389